An Analysis of the Performance of the UFAM Pulsed Doppler Lidar for Observing the Boundary Layer

GUY PEARSON

School of Environment and Life Science, University of Salford, Salford, and Halo Photonics Ltd., Leigh, United Kingdom

FAY DAVIES AND CHRIS COLLIER

School of Environment and Life Science, University of Salford, Salford, United Kingdom

(Manuscript received 3 March 2008, in final form 21 July 2008)

ABSTRACT

The performance of the 1.5-μm pulsed Doppler lidar, operated by the U.K. Universities Facility for Atmospheric Measurement (UFAM) over a 51-day continuous and unattended field deployment in southern England, is described and analyzed with a view to demonstrating the capabilities of the system for remote measurements of aerosols and velocities in the boundary layer. A statistical assessment of the vertical pointing mode in terms of the availability and errors in the data versus range is presented. Examples of lidar data are compared to theoretical predictions, radiosondes, the UFAM radar wind profiler, and an ultrasonic anemometer.

1. Introduction

Real-time and continuous observations of the lower levels of the atmosphere can provide timely information for now- and forecasting local weather, pollution levels, visibility, cloud characteristics, and wind. In addition, long-term observations of the dynamics and particulate levels in urban and rural environments offer a valuable climatological record with uses in predicting and analyzing phenomena such as convection, waves, dispersion of pollution, wind resource availability, and mesoscale meteorology in general (Collier et al. 2005; Davies et al. 2007; Middleton and Davies 2005; Newsom and Banta 2003; Frehlich et al. 2006; Spuler and Mayor 2005). Traditional point sampling instrumentation provides data at or near ground level but observations of the 3D velocity field, turbulence, and the particulate matter with diameters of 2.5 μm or less (PM2.5) count throughout the boundary layer have to date only been available sporadically using towers or tethered balloons.

Pulsed Doppler lidar (Huffaker and Hardesty 1996; Grund et al. 2001), the optical analog of Doppler radar, is a remote sensing technology that has now developed past bespoke systems operated by research organizations to the point where meteorological end users can operate commercially available instruments for long-term, autonomous deployments. Instruments of this type have the capability to remotely measure the dynamics and particulate levels in the atmosphere and have the attractive features of silent operation and small size. In addition they do not suffer from interference and have no ground clutter problems. Naturally occurring aerosols and clouds backscatter the transmitted pulses of near-infrared radiation. The Doppler shift imparted on the backscattered light is proportional to the line-of-sight component of the scatterers' velocity. The motion of the aerosols and cloud particles can therefore be analyzed remotely. The strength of the aerosol return signal depends upon the amount of suitable aerosol in the atmosphere and this is known to be dependent upon geographic location, the condition of the atmosphere, and the synoptic situation. The degree to which lidars of this type are all-weather is elucidated by the dataset presented here. Within the context of the aerosol number density, precipitation has a purging effect that usually results in a temporary reduction in the operational range immediately following rain. The lidar detects rain, liquid water clouds, mixed phase clouds, and ice clouds. The penetration depth into cloud

Corresponding author address: Guy Pearson, Peel Building, University of Salford, Salford M5 4WT, United Kingdom.
E-mail: guy@halo-photonics.com

DOI: 10.1175/2008JTECHA1128.1

TABLE 1. Parameters of the lidar.

Wavelength	1.5 μm
Pulse repetition rate	20 kHz
Bandwidth (B)	± 14 m s^{-1}
Sampling frequency	30 MHz
Points per range gate (M)	6
Number of pulses averaged (n)	20 000
Δr	18 m
Δp	30 m
Averaging time	1 s

varies between 100 m and several kilometers for liquid water and mixed phase clouds, respectively. The data presented here are primarily from aerosol returns.

Important factors for meteorological users of a Doppler lidar are the statistics of the achievable ranges and Doppler measurement accuracies in typical atmospheric conditions. To address these issues we have carried out a continuous data collection over a 51-day period at a location in southern England with a compact, commercially available instrument. While this does not represent the long-term study that would be required for a full analysis of these factors, the intention was to provide some information on the performance that can be expected for this region and to compare the results from the lidar with more established technologies: radiosondes, radar, and ultrasonic anemometers.

The instrument was manufactured by Halo Photonics Ltd. and is part of the U.K. Universities Facility for Atmospheric Measurement (UFAM) instrument pool. It has previously been deployed to the Helsinki test bed (Bozier et al. 2007) and the Convective and Orographically Induced Precipitation Study (COPS) in southern Germany (Wulfweyer et al. 2008).

2. Instrument description and predicted performance

The instrument is a self-contained, air-cooled module similar in size to a desktop personal computer and utilizes contemporary fiber-optic components (Pearson et al. 2002; Kameyama et al. 2007). The system requires 150 W of electrical power and the field-of-view of the instrument can be scanned anywhere within a 2π steradian field-of-regard using a two-axis scanner. The principle parameters of the instrument are shown in Table 1. Here we use the range gate parameters, Δr and Δp (Frehlich 2001), where the former relates to the pulse length and the latter is the downrange extent of the range gate used in the signal processing. The pulse rate of 20 kHz gives a maximum unambiguous range of 7.5 km but data were only recorded out to a range of 3 km for this deployment.

There have been a number of studies on the performance of Doppler estimation algorithms for this application (Frehlich et al. 1997; Frehlich 2001, 2004; Rye and Hardesty 1993, 1997; Dabas 1999). However, little experimental work has been done in the low-pulse energy, high–pulse rate mode employed by this instrument. The two parameters of importance for end users are the threshold wideband signal to noise ratio (SNR) for reliable data and the standard deviation of the Doppler measurements. Doppler measurements from distributed incoherent scattering using heterodyne lidars of this type are known to depart from the theoretical limit applicable to direct detection systems. This issue has been examined in detail by Rye and Hardesty (1997). The regime of interest here is where the weak returns from many pulses are accumulated prior to estimating the Doppler information. The two parameters important in predicting the performance in this mode are α and the SNR; α is a dimensionless parameter that characterizes the ratio of the photon count to the speckle count and is linked to the system parameters by the relation,

$$\alpha = \mathrm{SNR}/\left[(2\pi)^{0.5}(\Delta\nu/B)\right], \tag{1}$$

where $\Delta\nu$ is the signal spectral width and B is the receiver bandwidth. For $\Delta r = 18$ m and a 1 m s^{-1} atmospheric broadening factor, $\Delta\nu \approx 1.5$ m s^{-1} and therefore for the parameter values of the UFAM lidar, α is approximately equal to $6 \times$ SNR.

The theoretical standard deviation of the Doppler estimate in the weak signal, multipulsed averaged regime can be approximated by the expression (Rye and Hardesty 1993)

$$\sigma\,(\mathrm{m\,s^{-1}}) = 2(\pi^{0.5}/\alpha)^{0.5}(1 + 0.16\alpha)(\Delta\nu/N_p^{0.5}), \tag{2}$$

where N_p is the accumulated photocount that is related to the SNR by

$$N_p = Mn(\mathrm{SNR}). \tag{3}$$

For a coherent lidar, Eq. (2) is not valid when the SNR values increase above -5 dB. At these SNR values, the speckle or fading on the signal leads to a saturation in the Doppler measurement. This is caused by the fact that even at high averaged photocounts, the rate of change in the phase through individual fades causes a frequency broadening that limits the attainable precision.

The heterodyne results from Eq. (2) can be compared to the limiting precision for an analogous direct detection that is simply given by

$$\sigma\,(\mathrm{m\,s^{-1}}) = \Delta\nu/N_p^{0.5}. \tag{4}$$

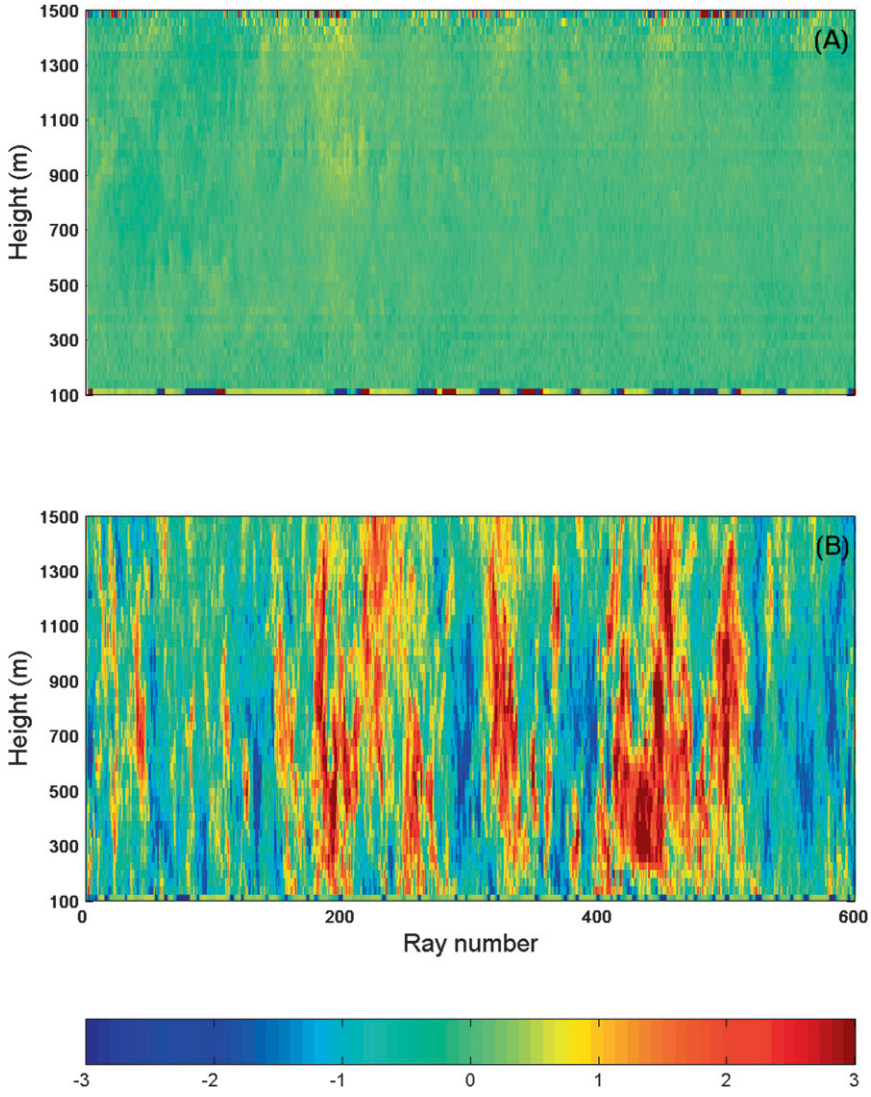

FIG. 1. Time vs height representation of the vertical velocity data from (a) stable evening (1900 UTC 11 Sep 2007) and (b) early afternoon convective periods (1300 UTC 10 Sep 2007) as observed at the Cardington site. For (a) and (b) the total observation time was 55 min and the vertical resolution was 30 m. Blue colors indicate downward motion.

For an SNR = −5 dB, Eq. (1) is within about a factor 2 of the direct detection limit. This factor increases to about 8 at an SNR = −20 dB. Values from these expressions are compared to the data in the following sections.

3. Description of deployment

For this data collection campaign, the instrument was installed in a vehicle that was located at the Met Office research establishment at Cardington, United Kingdom (latitude: 52.12°N, longitude: 0.4°E).

The lidar was nominally scheduled to perform a set sequence of measurements per hour although this schedule was adjusted (remotely over the Internet) occasionally when interesting atmospheric conditions were expected. The schedule consisted of taking a conical scan (fixed 60° elevation, azimuth 0°–360°) on the hour and staring vertically for the remainder of the hour. The scanner was operated in a step-stare mode with the data being acquired during the static staring periods. The hourly conical scans consisted of 72 lines of sight and took approximately 9 min to execute.

For the duration of the deployment the 1290-MHz, Degreane UFAM radar wind profiler (Norton et al. 2006) was collocated with the lidar, and radiosondes (Vaisala RS92-SGPW) were periodically launched from the site. Examples of contemporaneous lidar, radar, and sonde wind profiles are shown in section 4(d).

4. Data analysis

a. Doppler measurement

The first parameter that we investigated was the error in the Doppler measurements. To characterize the Doppler errors we identified the subset of data for which the vertical velocity field was close to zero and relatively constant versus range and time (over a 20-min period). These periods were typically in the evening and at night. An example of the vertical velocity versus height and time for these conditions is shown in Fig. 1a. This is in contrast to the data in Fig. 1b that show turbulent plumes indicative of convective activity in mid-afternoon. For the conditions shown in Fig. 1a, it is reasonable to assume that the observed errors in the measurements of vertical velocity were instrumental and due to the statistical uncertainty in estimating the velocity from the averaged range-gate spectra.

In terms of the velocity measurement precision, the two parameters of interest are the bias and standard deviation. The possibility of a bias was investigated by analyzing multiple 1-h-long records of vertical velocity (1-s average) for periods when there was no convection, since in this case the average vertical velocity should be close to zero. We found that the average vertical velocity for these 1-h-long records was consistently within ± 2 cm^{-1} of zero, indicating that there was minimal bias in the velocity measurements.

To quantify the errors in the Doppler measurements, the experimentally observed standard deviation, σ, of the vertical velocity as a function of the SNR was evaluated. The autocorrelation scheme (Frehlich 2001) was used to evaluate the errors since it has been shown to produce good results in this regime. This time domain analysis allows determination of the uncorrelated (random) component of the variation between the sequential measurements. The difference between the first term in the autocorrelation, the zeroth lag (proportional to the sum of the squares of the individual estimates), and the second term (proportional to the sum of the products of adjacent measurements) gives a measure of the random error in the velocity time series. Examples of the time series and their respective autocorrelations for two different SNRs of -12 and -19 dB are shown in Figs. 2a,b. The SNR used throughout the analysis is the wideband SNR as determined from the time domain records of range-gated return power. Figure 2c shows the standard deviations (σ), as evaluated from the zeroth lag impulse in the autocorrelation, for 256 individual, 9.5-min-long records of the vertical velocity. Here the σ values are plotted versus SNR and compared to points generated by Eqs. (2) and (4). In the high-SNR region, the errors are constant (at about 3–4 cm^{-1}) because of the effect of the speckle-induced phase noise alluded to earlier. At reduced values of the SNR, the errors increase, rising to approximately 40 cm^{-1} at an SNR $= -20$ dB. It can be seen that in the region where it would be expected, the experimental data are well clustered about the values of Eq. (1). We have found experimentally that the threshold SNR for reliable data is on the order of -23 dB. This can be approximately interpreted as the experimentally determined SNR threshold above which the probability of

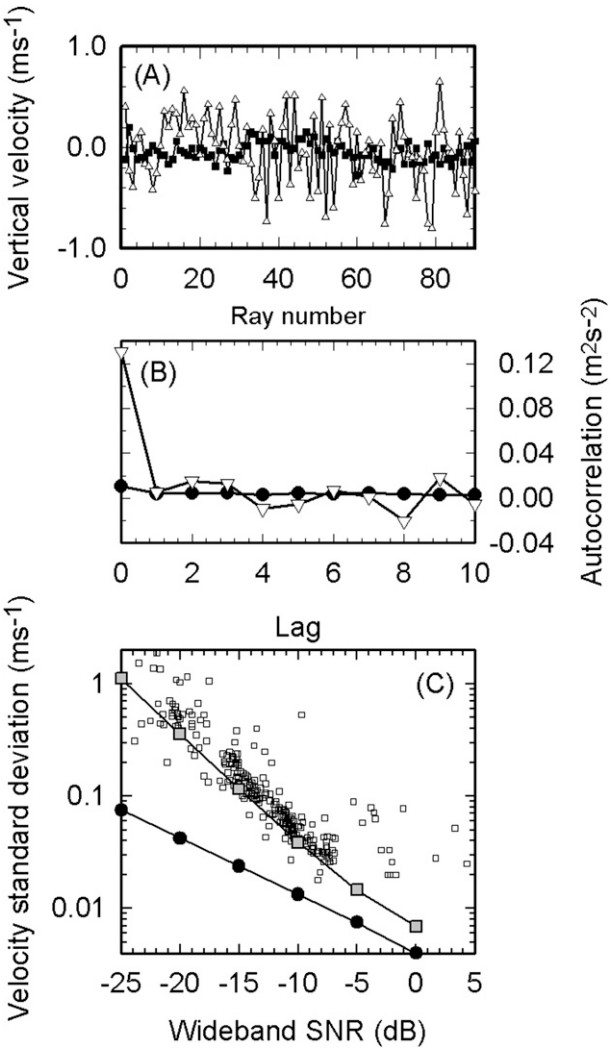

FIG. 2. (a) Two vertical velocity time series for two range gates observed during stable conditions. The wideband SNRs for the solid square and open triangle datasets were -12 and -19 dB, respectively. (b) The autocorrelation functions of the two times series shown in (a). The impulse of the zeroth lag indicates the random error and in the two examples shown corresponds to 0.36 m s^{-1} (open triangles) and 0.10 m s^{-1} (solid circles). (c) The errors calculated from 256 individual records of this type vs SNR (open symbols). The gray squares show the values calculated using Eq. (2). The solid circles show the limiting case of Eq. (4).

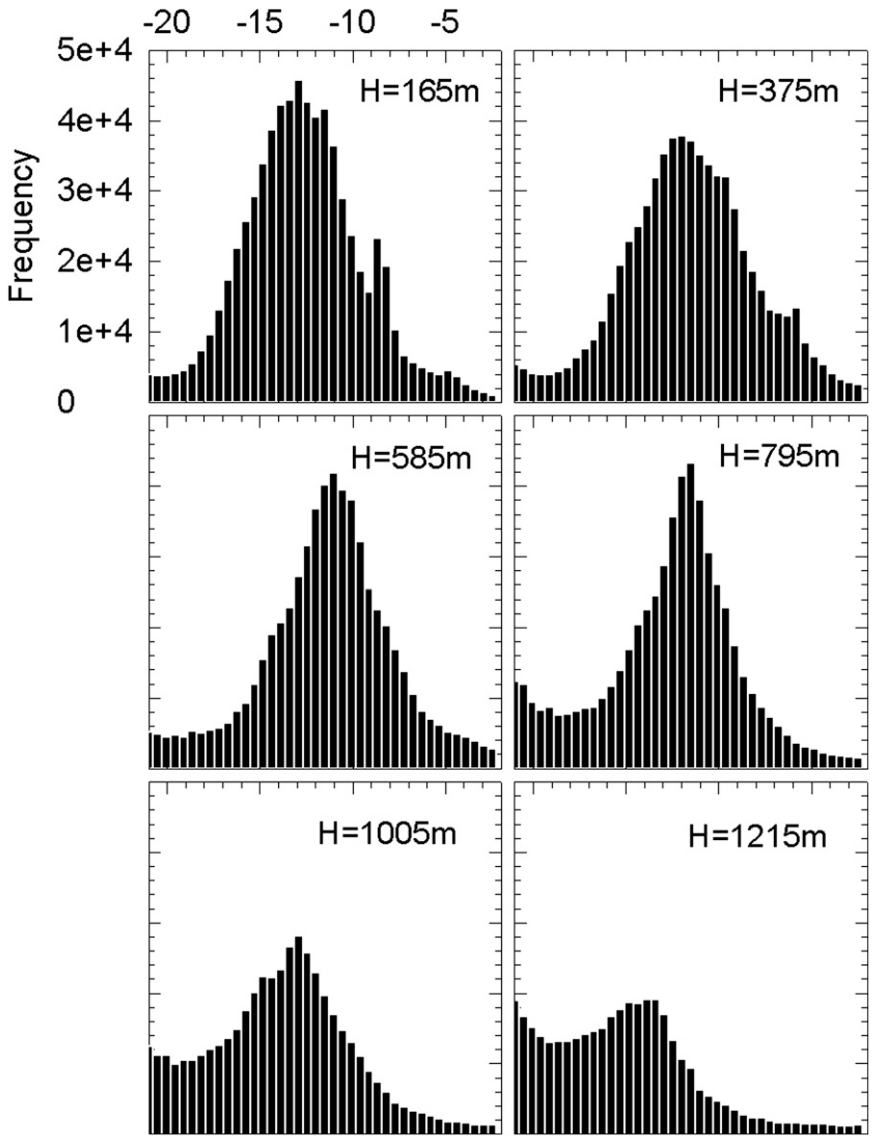

FIG. 3. Histograms showing the distribution of the SNR for six individual 30-m range gates located at the stated altitudes. The whole 51-day dataset was analyzed and cloud was excluded by thresholding the data at an SNR of −2 dB.

a false Doppler estimate is less than 5%. Predictions of this threshold have been published previously by Kameyama et al. 2007, Rye and Hardesty 1993, and Dabas 1999 and appear to be in reasonable agreement with this experimentally observed result.

b. SNR statistics

The variations in the aerosol loading of the lower atmosphere influence the SNR versus height. It has been qualitatively shown previously (Bozier et al. 2007) that the lidar backscatter coefficient is correlated to the PM2.5 count as determined by point sampling instrumentation. Therefore, records of this parameter may be useful in predicting the performance of the lidar in other locations. The only reliable method of assessing the variability of the aerosol versus time and height in a given location is to collect datasets over an extended period. The frequency of precipitation, the back trajectory of the air mass, and the season are all factors that are known to influence the aerosol concentration (Spinhirne et al. 1997; Srivastava et al. 2001; Vaughan et al. 2002). The observed SNR versus height for the complete vertically staring dataset was analyzed and Fig. 3 shows the essential features with reference to six range gates centered at altitudes (above ground level) of 165, 375, 585, 795, 1005, and 1215 m. The data were

filtered with respect to the SNR in order to disregard returns from cloud. By examining the data it was found that a suitable threshold was −2 dB, and data where the SNR values were greater than this were ignored. For range gate 5, centered at a height of 165 m, the mean, median, and interquartile range for the SNR dataset were −11.4, −13, and (−15 to −11 dB), respectively. The velocity errors associated with the SNR distributions shown in Fig. 3 can be estimated from Fig. 2c. For example, the median SNR value of −13 dB for gate 5 corresponds to a velocity standard deviation on the order of 7 cm^{-1}.

c. Range for vertical velocity measurements

The height to which the instrument operates in a vertical mode is dependent upon the setup of the instrument and the atmospheric conditions. The important parameters with respect to the atmosphere are the aerosol concentration versus height and the cloud cover. The aerosol backscatter is typically higher in the boundary layer with an order of magnitude or greater reduction being common at the transition to the free troposphere. The lidar was designed so that it would have sufficient sensitivity to reliably detect returns from the entire boundary layer. Since the backscatter falls sharply at the top of the boundary layer, consistent data into the free troposphere can only be assured by a discontinuous step up in lidar sensitivity, which typically comes with additional complexity and a loss of the autonomous and compact attributes of the UFAM system. The statistics of the height to which vertical measurements were obtained, as discussed in the following section, are well correlated with the boundary layer height (BLH), as defined by the height at which there is a strong negative gradient in the backscatter. The correlation of the BLH as defined in this way, the potential temperature definition and the predictions of models, has been studied previously (Davies et al. 2007)

On occasions there were additional higher layers of aerosol but the analysis below was performed on the basis of the height to which there was continuous data. An interesting feature of the Doppler lidar data is that at nighttime (when there may be a residual classical boundary layer height of several hundred meters as defined by the backscatter gradient), the height to which vertical transport occurs can be separately determined, giving a better estimate of the effective nighttime boundary layer (or mixing) height.

To evaluate the performance of the lidar for profiling vertical velocity and aerosol concentration in the lower layer of the atmosphere, the maximum height to which continuous data were available was extracted from the whole data record. For sequential 30-min-long sections of the whole dataset, the average height to which continuous data were available was evaluated. In addition, for each case, it was recorded whether or not the maximum range was limited by cloud. In total, 2077 individual measurements were derived from the data and a probabilistic representation of these data is shown in Fig. 4. It was determined that 52% of the time, cloud limited the maximum range, and 14% of the time this cloud was at an altitude of 500 m or less. For the cloud-free data, 95% of the time the instrument operated up to 700 m. When the whole dataset was considered, the corresponding number was 82%. The 50% probability height was approximately 1100 m for both the combined and cloud-free datasets. For this data collection period, only about 4 h worth of data were lost due to heavy rain. The instrument detects a return from rain but no signal is detected when heavy rain temporarily pools on the output window.

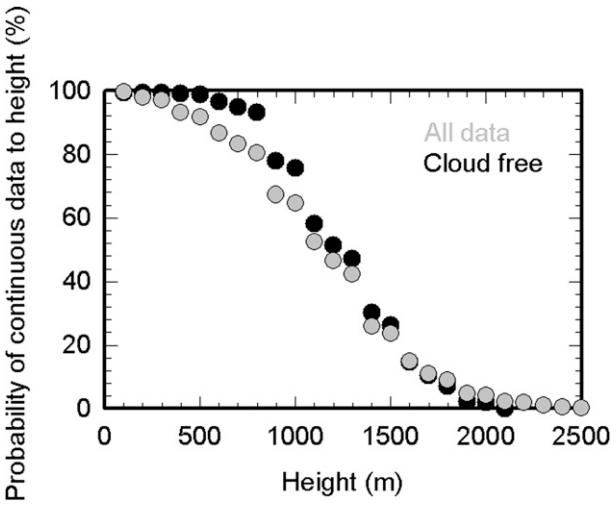

FIG. 4. The probability of continuous data from the ground up to a given height over the 51-day period.

From Fig. 3, it is possible to estimate the near-horizontal range performance that would have been obtained with the lidar during this deployment. When the system sensitivity versus range is taken in conjunction with the observed boundary layer SNR statistics, the calculated probabilities of observing to near-horizontal ranges of 3 and 5 km are approximately 90% and 50%, respectively.

d. Wind profiling

One of the applications of this instrument is boundary layer wind profiling. There are two modes that can be utilized for this. The beam can be scanned in a cone at fixed elevation and the resulting data fitted to a sine wave [velocity–azimuth display (VAD) approach; Browning and Wexler 1968] or three fixed line of sights

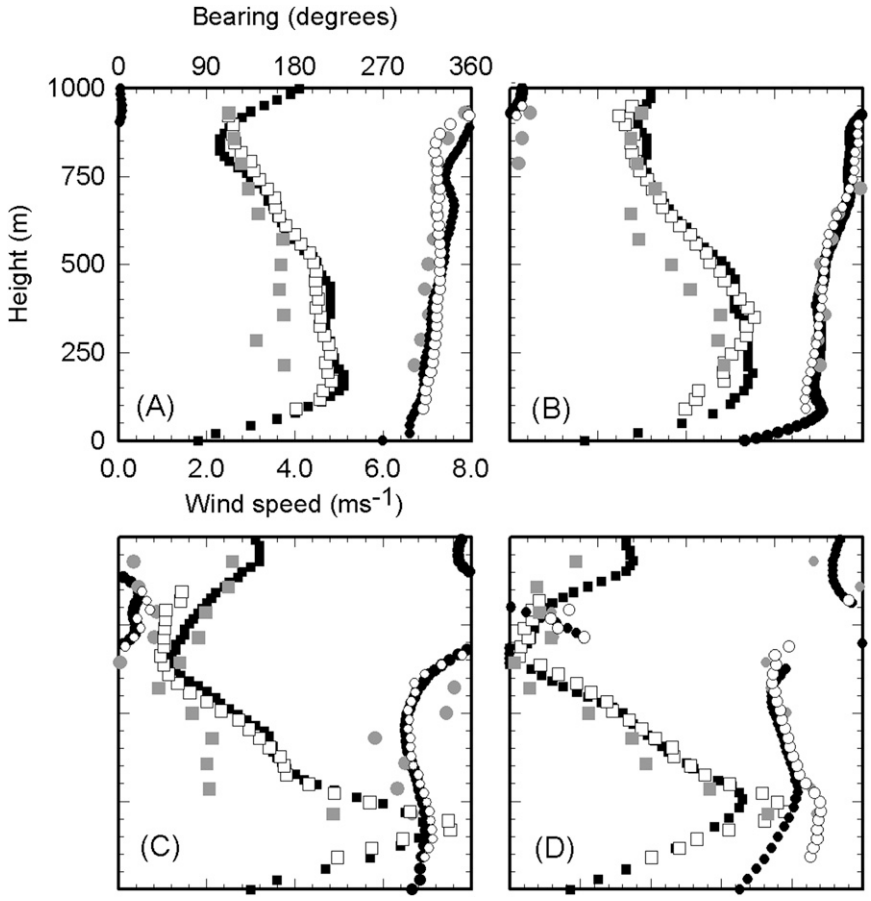

FIG. 5. Wind profiles obtained using three separate instruments through the evening of 7 Sep 2007. The black, open, and gray symbols show data from radiosondes, lidar, and radar, respectively. The squares show speed and the circles bearing. (a)–(d) Radar and lidar data (10-min average, starting on the hour) at 1900, 2000, 2100, and 2200. The radiosonde launch times were 1922, 1953, 2056, and 2156. Every fourth point is shown for the radiosonde data to avoid cluttering the plot.

can be recorded followed by a vector analysis to yield the three components of the wind (u, v, and w) (Werner 2005). The three-beam technique may offer a better option in regions where the flow is not constant and laminar over the disc swept out by the VAD scan. This is of particular relevance for regions where topographic features influence the flow field. In addition, it offers a wind profiling capability where site conditions are such that there is a restricted field-of-view that prohibits access to a full range of azimuth angles. Here we show examples of both approaches and compare the data to profiles derived from radiosondes and the UFAM radar wind profiler.

Figure 5 shows the results from an intercomparison carried out on 7 September 2007. The scanner operated in a conically scanned, step-stare mode, looking along each line of sight for 1 s. The elevation angle was 60° and the azimuth step was 5° (72 points) and the full scan took approximately 9 min to complete. In this case, for all heights up to the cloud base, the coefficient of variation (defined as the standard error/parameter value) reported by the sine-wave fit algorithm used to derive the bearing and speed parameters from the scanned data was <1.5%. The same data were decimated by various factors and reanalyzed in order to observe the effects of fewer points on the sine-wave fit. For 18 and 6 equally spaced points, the errors only increased to 2% and 3%, respectively.

The radiosonde measurements tend to show the influence of gusts and spatial variability whereas the VAD approach is averaging the atmosphere over a spatial scale of hundreds of meters (the diameter of the disc swept out during the measurement) and a time scale of 9 min.

A series of four radiosondes were launched during this period and these data are overplotted in Fig. 5.

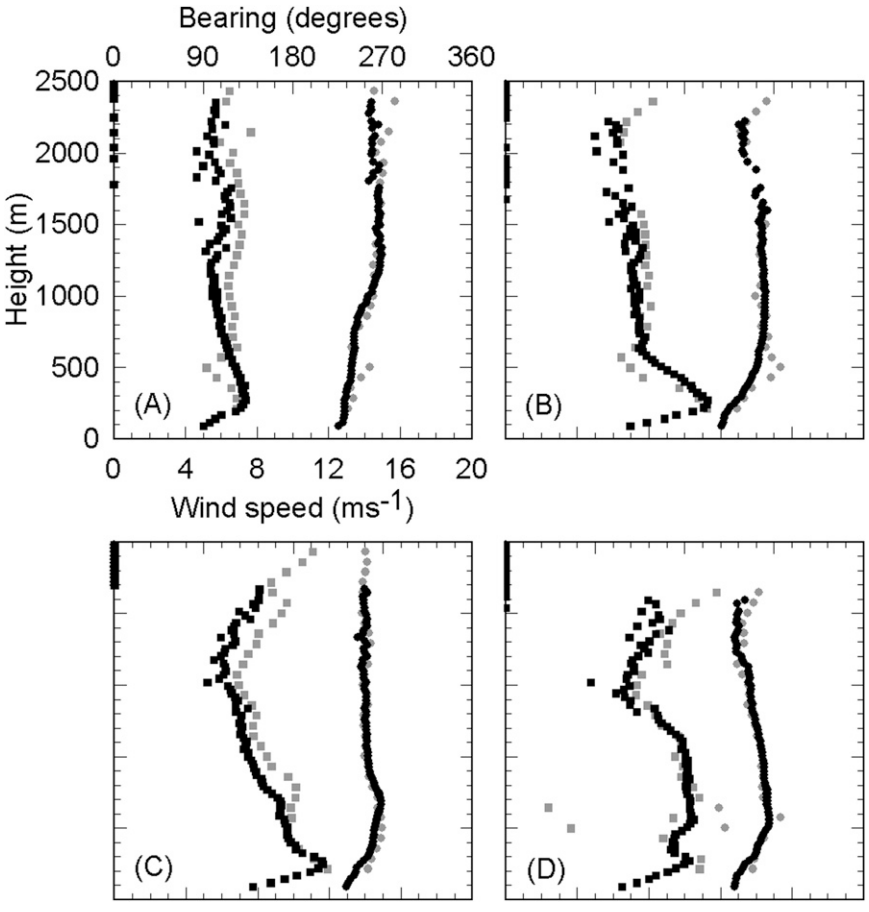

FIG. 6. Radar and lidar profiles from the evening of 13 Sep 2007. The lidar scan took 9 min and the radar data are for a 10-min average. (a)–(d) Start times of 1900, 2100, 2200, and 2300 UTC, respectively. The circles and squares show the bearing and speed data, respectively (gray radar and black lidar).

There was a layer of cloud at about 900-m altitude that gradually descended as the evening progressed. A low-level flow at higher speed also developed during the course of the evening. It can be seen that the lidar and radiosonde measurements are highly correlated with both the bearing and speed values, showing a good level of agreement. Ten-minute averaged data from the UFAM radar wind profiler are also shown in Fig. 5. This device operates with three fixed lines of sight, one vertical and two orthogonal (in azimuth), and inclined to the vertical at 17°. The range resolution for the radar data was 70 m and the beamwidth was 8.5°.

When assessing the level of agreement between the instruments that should be expected, the different spatial and temporal characteristics of the measurements must be considered within the context of the spatial and temporal characteristics of the prevailing atmospheric dynamics. The radar velocity data show some discrepancies with the lidar and sonde data. The radar was averaging for approximately the same time period as the lidar but over a narrowed (horizontally) and extended (vertically) volume of the atmosphere. In addition it is possible that insects and ground clutter were influencing the radar data.

Figure 6 shows radar and lidar profiles from the evening of 13 September 2007. There was no cloud cover during the evening and the entrained aerosol had been elevated up to an altitude of around 2 km by the convective activity in the afternoon. At an altitude of about 1200 m the backscatter versus height exhibited a negative gradient that can be seen in the data by way of a slight increase in the scatter of both the speed and bearing data. This is because resulting reduction in the SNR leads to a larger degree of uncertainty in the sine-wave fit procedure. The radar and lidar bearing data show a very good level of agreement. Again, the wind speed data are less well correlated, similar behavior to that observed on the evening of the 7th. Further work

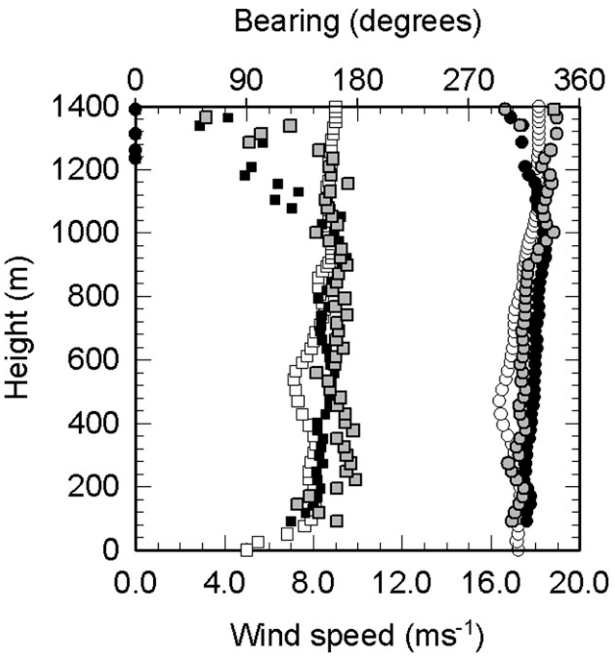

FIG. 7. Radiosonde and lidar-derived wind profiles from 7 Sep 2007. The squares and circles correspond to the speed and bearing axes, respectively. The solid black symbols are derived from a VAD scan starting at 1500. The gray symbols are for a three-beam sequence of data taken at 1509. The open symbols are the radiosonde data with a launch time of 1533.

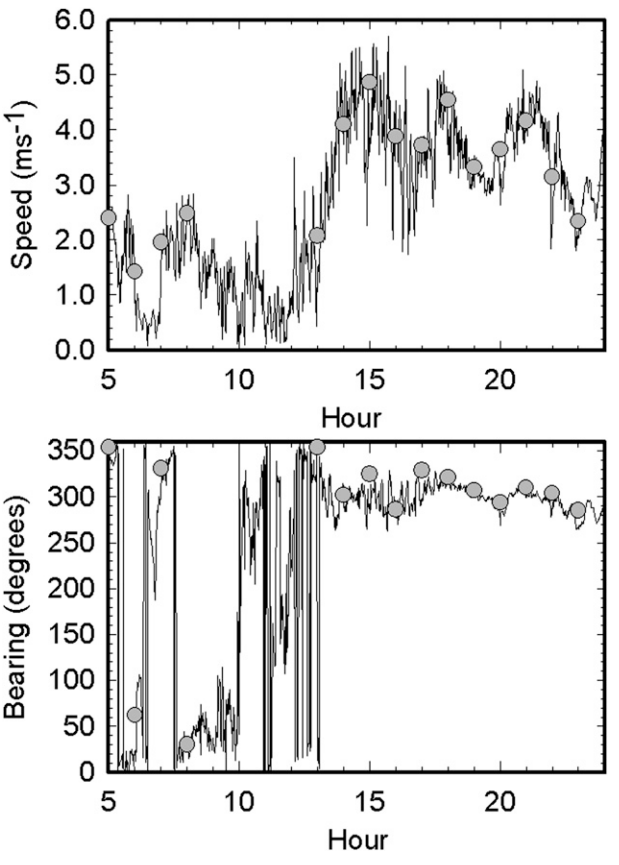

FIG. 8. An example of hourly (top) speed and (bottom) bearing from the lowest lidar range gate (gray circles) vs a sonic anemometer mounted on a collocated tower (100 m away).

will investigate this issue and also investigate whether ground clutter is contaminating the radar velocity data.

Figure 7 shows lidar and radiosonde data from the afternoon of 7 September 2007. A radiosonde was launched at 1533 from the Cardington site and the open symbols show the speed and bearing wind data. Starting at 1500 the lidar performed a similar conical scan to that described earlier with reference to Fig. 5. At 1509, the lidar performed a three-beam wind profile by sequentially probing three fixed lines of sight (1: vertical, 2: 205° azimuth, 60° elevation, and 3: 295° azimuth, 60° elevation). The different spatial and temporal resolutions of these measurements must again be considered when interpreting these data. The lidar profiles derived from the conically scanned and three-beam data differ in their total observation times of the atmosphere by a factor of 24 and therefore the increased scatter of the three-beam data is to be expected. A detailed intercomparison of the conical scanned and three-beam approaches requires an analysis of their respective behaviors versus averaging time and SNR. The influence of the smoothing and assumptions inherent in the sine-wave fit procedure must also be factored in particularly when analyzing complex flow situations. An analysis of these factors will be presented in a future report. However, these data are included here to emphasize the point that the lidar system is capable of providing wind profile data throughout the boundary layer with an update rate of three or more profiles per minute.

Figure 8 shows an example of hourly lidar speed and bearing data (derived from a 9-min conical scan) overplotted with data from a tower-mounted ultrasonic anemometer for 7 September 2007. The tower was located about 100 m from the lidar. Again, it can be seen that the two measurements show a good level of correlation.

5. Summary and conclusions

To parameterize the operational characteristics of the new UFAM pulsed Doppler lidar instrument, a set of data, acquired in a continuous and autonomous mode at a site in southern England over a 51-day period in late summer 2007, has been analyzed. The instrumental error in the Doppler measurements has been analyzed by assessing the random contribution to time series of the vertical velocity acquired during stable conditions. These data, taken in conjunction with the histograms showing the observed distribution of the SNR versus

height over the 51-day period, allow estimates of the expected errors in the vertical velocity measurements to be determined. The values obtained show that in the atmospheric boundary layer, error of <10 cm^{-1} can be expected from the instrument. These values are sufficiently low that it is feasible to analyze the data further to extract detail such as the eddy dissipation rate, an important parameter difficult to measure by any other technique.

The statistics of the height to which continuous measurements could be made and the fraction of the time clouds limited by the maximum range allow some assessment to be made of the utility of the instrument for meteorological observations. Over the period of the study, the inherent sensitivity of the instrument was always sufficient to detect returns from the aerosol entrained in the boundary layer. The statistics of the maximum height for data are effectively the statistics for the boundary layer height as determined by the gradient in the backscatter versus height profile. However, alternative definitions of the boundary layer height are possible for a Doppler instrument based upon the height to which vertical transport or turbulence are active.

The lidar-derived wind profiles have been compared to radiosonde, radar, and ultrasonic anemometer data and in general, the agreements have been shown to be qualitatively very good although there exist some discrepancies in the radar–lidar correlations that warrant further investigations.

It is currently not possible to quote the absolute backscatter from this particular instrument but in the future this will be possible and the high level of stability and repeatability of the instrument will permit the data presented here to be inverted for absolute backscatter values.

It is recognized that the performance levels observed are dictated by the aerosol loading and can therefore not be assumed to be in any way universal with respect to location. In addition, the location was relatively rural. However, in terms of extrapolating the performance to other midlatitude environments, the 51-day sample is long enough to give some validity to the statistics. The prevailing wind direction over the United Kingdom is southwesterly, resulting in a bias to maritime-type air masses. It would be expected that this tends to result in relatively clean air advecting over the country. Continental or urban locations may offer enhanced levels of performance. Indeed, recent data collected in central London have shown higher SNR values.

Acknowledgments. The authors thank Jeremy Price (Met Office) for authorizing and facilitating the deployment at Cardington and Amanda Kerr Munslow (Met Office) and Emily Norton (University of Manchester) for kindly providing the radiosonde, sonic anemometer, and radar data.

REFERENCES

Bozier, K. E., G. N. Pearson, and C. G. Collier, 2007: Doppler lidar observations of Russian forest fire plumes over Helsinki. *Weather,* **62,** 203–208.

Browning, K. A., and R. Wexler, 1968: The determination of kinematic properties of a wind field using Doppler radar. *J. Appl. Meteor.,* **7,** 105–113.

Collier, C. G., and Coauthors, 2005: Dual-Doppler lidar measurements for improving dispersion models. *Bull. Amer. Meteor. Soc.,* **86,** 825–838.

Dabas, A., 1999: Semi-empirical model for the reliability of a matched filter frequency estimator for Doppler lidar. *J. Atmos. Oceanic Technol.,* **16,** 19–28.

Davies, F., D. R. Middleton, and K. E. Bozier, 2007: Urban air pollution modeling and measurements of boundary layer height. *Atmos. Environ.,* **41,** 4040–4049.

Frehlich, R., 2001: Estimation of velocity error for Doppler lidar measurements. *J. Atmos. Oceanic Technol.,* **18,** 1628–1639.

——, 2004: Velocity error for coherent Doppler lidar with pulse accumulation. *J. Atmos. Oceanic Technol.,* **21,** 905–920.

——, S. M. Hannon, and S. W. Henderson, 1997: Coherent Doppler lidar measurements of winds in the weak signal regime. *Appl. Opt.,* **36,** 3491–3499.

——, Y. Meillier, M. L. Jensen, and B. Balsley, 2006: Measurements of boundary layer profiles in an urban environment. *J. Appl. Meteor. Climatol.,* **45,** 821–837.

Grund, C. J., R. M. Banta, J. L. George, J. N. Howell, M. J. Post, R. A. Richter, and A. M. Weickmann, 2001: High-resolution Doppler lidar for boundary layer and cloud research. *J. Atmos. Oceanic Technol.,* **18,** 376–393.

Huffaker, M. R., and R. M. Hardesty, 1996: Remote sensing of atmospheric wind velocities using solid state and CO_2 coherent laser systems. *Proc. IEEE,* **84,** 181–204.

Kameyama, S., T. Ando, K. Asaka, Y. Hirano, and S. Wadaka, 2007: Compact all-fiber pulsed coherent Doppler lidar system for wind sensing. *Appl. Opt.,* **46,** 1953–1962.

Middleton, D. R., and F. Davies, 2005: Evaluation of dispersion model parameters by dual Doppler lidars over West London, England. *Int. J. Environ. Pollut.,* **25,** 80–88.

Newsom, R. K., and R. M. Banta, 2003: Shear flow instability in the stable nocturnal boundary layer as observed by Doppler lidar during CASES-99. *J. Atmos. Sci.,* **60,** 16–33.

Norton, E. G., G. Vaughan, J. Methven, H. Coe, B. Brooks, M. Gallagher, and I. Longley, 2006: Boundary layer structure and decoupling from synoptic scale flow during NAMBLEX. *Atmos. Chem. Phys.,* **6,** 433–444.

Pearson, G. N., P. J. Roberts, J. R. Eacock, and M. Harris, 2002: Analysis of the performance of a coherent pulsed fiber lidar for aerosol backscatter applications. *Appl. Opt.,* **41,** 6442–6450.

Rye, B. J., and R. M. Hardesty, 1993: Discrete spectral peak estimation in incoherent backscatter heterodyne lidar. II: Correlogram accumulation. *IEEE Trans. Geosci. Remote Sens.,* **31,** 28–35.

——, and ——, 1997: Estimate optimization parameters for incoherent backscatter heterodyne lidar. *Appl. Opt.,* **36,** 9426–9436.

Spinhirne, J. D., S. Chudamani, J. F. Cavanaugh, and J. L. Bufton, 1997: Aerosol and cloud backscatter at 1.06, 1.54, and 0.53 μm by airborne hard-target-calibrated Nd:YAG /methane Raman lidar. *Appl. Opt.,* **36,** 3475–3490.

Spuler, S. M., and S. D. Mayor, 2005: Scanning eye-safe elastic backscatter lidar at 1.54 μm. *J. Atmos. Oceanic Technol.,* **22,** 696–703.

Srivastava, S., and Coauthors, 2001: Wavelength dependence of backscatter by use of aerosol microphysics and lidar data sets: Application to 2.1-μm wavelength for space-based and airborne lidars. *Appl. Opt.,* **40,** 4759–4769.

Vaughan, J. M., R. H. Maryon, and N. J. Geddes, 2002: Comparison of atmospheric aerosol backscatter and air mass back trajectories. *Meteor. Atmos. Phys.,* **79,** 33–46.

Werner, C., 2005: Doppler wind lidar. *Lidar: Range-Resolved Optical Remote Sensing of the Atmosphere,* C. Weitkamp, Ed., Series in Optical Sciences, Vol. 102, Springer, 339–342.

Wulfmeyer, V., and Coauthors, 2008: The Convective and Orographically Induced Precipitation Study (COPS): A research project for improving quantitative precipitation forecasting in low-mountain regions. *Bull. Amer. Meteor. Soc.,* **89,** 1477–1486.